Additive Manufacturing 62 (2023) 103373



Contents lists available at ScienceDirect

Additive Manufacturing

journal homepage: www.elsevier.com/locate/addma

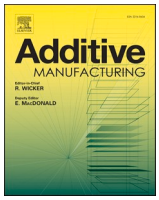

Research paper

Continuous 3D printing of microstructured multifunctional materials



Lizhi Guan [a], Jingbo Fan [b], Xin Ying Chan [a], Hortense Le Ferrand [a,b,c,*]

[a] School of Mechanical and Aerospace Engineering, Nanyang Technological University, 639798, Singapore
[b] School of Materials Science and Engineering, Nanyang Technological University of Singapore, 50 Nanyang Avenue, 639798, Singapore
[c] Singapore Centre for 3D printing, Nanyang Technological University of Singapore, 50 Nanyang Avenue, 639798, Singapore

ARTICLE INFO

Keywords:
3D printing
Magnetic field, microstructured materials
Anisotropy
Local orientation

ABSTRACT

Microstructured materials are promising for achieving as-designed local properties, enhanced global properties, and multifunctionality. Here, we developed an extrusion-based 3D printing method called magnetic direct ink writing (M-DIW), that continuously printed materials with local orientation of 2D microparticles at high concentration, using magnetic fields below 100 mT. The printing is enabled by carefully designing the viscosity of the inks to allow the same time extrusion and microparticle motion. This is realized by adjusting the magnetic functionalization of the microplatelets, adding a small concentration of fumed silica, and finding the optimum solid loading to obtain yield stress below 45 Pa. Proof-of-concept inks containing alumina and graphite microplatelets can be turned into a ceramic with an anisotropic flexural strength ranging 100–150 MPa after sintering, or composites with anisotropic conductivity ranging 5–25 S/m. Magnetically controlled electrical switches or self-shaping ceramics can be printed using M-DIW, for example.

1. Introduction

Microstructure in materials is known to enhance their properties. For example, orienting stiff inclusions in composites creates anisotropy with higher stiffness in the direction of the inclusions. Similarly, aligning conductive particles can create anisotropic conductivity. These properties are further enhanced when the inclusions or particles are present in high concentrations leading to percolating networks. For example, orienting BN microplatelets in high concentrations led to composites with ultra-high thermal conductivity along the direction of the alignment [1]. Similarly, orienting ceramic microplatelets in composites tailored their mechanical properties, including wear, hardness, stiffness, etc. depending on their orientation.[2] Even better than single orientations, locally microstructured materials can trigger other properties, such as self-shaping [3], impact resistance [4], combinations of strength and toughness [5], and so on. Such complex microstructures can be inspired by nature and leveraged to create new multifunctional materials [6]. A large variety of methods like freeze-casting [7], self-assembly [8], wet-spinning [9], vacuum filtration [10], centrifugation [11], shear force [12], electrical [13], and magnetic field [2] have been used to microstructure materials. However, those technologies are limited in terms of local microstructure control and macroscopic shaping with often one method being efficient for only one type of orientation, composition, and shape. To achieve materials of various compositions with as-designed properties through microstructure, in 3D shapes, and with time and cost-efficiency, a more general technology is desirable.

3D printing is a typical method to create tailored materials with time and cost-efficiency. 3D printing techniques including but not limited to stereolithography (SLA), extrusion-based direct ink writing (DIW), inkjet printing, and powder-bed fusion offer very effective ways of fabricating 3D structures with a large diversity of dimensions using a variety of materials [14,15]. To 3D print microstructured composites, external forces e.g., shear force, acoustic, magnetic, and electrical field have been used, leading to advances for applications in reinforced structural materials, tissue engineering, energy storage, soft robotics [16]. For instance, nanofibers or platelets suspended in an ink can align along with the flow direction due to the shear forces in the nozzle during extrusion-based 3D printing [17,18]. Instead of shear force, applying an electrical field in SLA is capable of aligning conductive anisotropic nanomaterials suspended in a resin to create complex structures such as biomimetic helicoidal microstructures.[19] Likewise, augmenting SLA with solenoids could induce local orientations to enhance the mechanical properties of composites [20]. However, despite these exciting advances in 3D printing techniques with microstructural control, a number of challenges remain. (i) Current methods are able to print microstructured composites containing a low particle concentration of up to

* Corresponding author at: School of Mechanical and Aerospace Engineering, Nanyang Technological University, 639798, Singapore.
E-mail address: hortense@ntu.edu.sg (H. Le Ferrand).

https://doi.org/10.1016/j.addma.2022.103373
Received 15 September 2022; Received in revised form 11 November 2022; Accepted 19 December 2022
Available online 20 December 2022
2214-8604/© 2022 Elsevier B.V. All rights reserved.

15 vol%, limiting the mechanical and functional properties that can be attained. (ii) Most microstructured materials that are 3D printed exhibit a single orientation throughout the composites which also limits the design of the functions of the materials. (iii) The methods able to control microparticles orientation in any direction in space do so in a step-by-step fashion that reduces the efficiency of the 3D printing in terms of speed and resolution. (iv) Most strategies have been applied to a single ink composition and have not demonstrated the possibility to vary the chemical composition in the ink.

To address these limitations, DIW combined with an external magnetic field is a possible approach. Indeed, DIW is based on the extrusion of a viscous ink through a nozzle and the deposition of this ink onto a print bed to build 3D structures in a layer-by-layer manner. Compared to other 3D printing techniques, a wide diversity of chemical compositions and the viscosities of the ink can be employed. Indeed, inks with high viscosity $>$ 1000 Pa·s can be directly printed, whereas inks with low viscosity, e.g., 5–150 Pa·s, can also be printed using a coagulation solution [21], a highly viscous supporting liquid [22], an absorbing porous substrate [23], or by freezing rapidly with ice support [24]. Since DIW can take various inks as input, it is a multimaterial printing method with diversity in compositions. Also, it can print composite materials with a high concentration in reinforcing particles. For example, DIW was used to print aqueous ink containing 21–24 vol% of calcium phosphate microplatelets [23]. Despite the high fluidity of the ink, shape-retention could be obtained by rapidly removing the water after the extrusion of the ink. Furthermore, in addition to the merits of DIW, applying external low magnetic fields is a low-cost, efficient and convenient approach to orient microparticles in any direction. Indeed, any anisotropic particle can be magnetized by ferromagnetic nanomaterials using a simple electrostatic interaction with superparamagnetic nanoparticles suspended in a ferrofluid, or using sol-gel chemistry to coat the particles [25]. After magnetic functionalization, particles of dimensions 1–50 μm approximately, exhibit ultra-high magnetic response allowing their quick alignment to magnetic fields strengths as low as 7 mT [26]. Recently, a multimaterial 3D printer coupled with a magnetic field was invented to control the alignment of magnetically-responsive microplatelets suspended in a monomer solution, in the vertical and horizontal directions [27]. In this method, every printed layer involved three steps including 2 min for the extrusion of the ink, 2 min for the magnetic alignment, and then 2 min for UV light curing of the polymeric matrix. In total, it took nearly 5 h for printing only 51 layers. Additionally, due to the use of UV light for curing, the concentration of the microplatelets was limited to 4 vol%. In turn, such low magnetic fields have shown the ability to orient microparticles in liquid slurries at concentrations up to 25 vol% [28]. By casting the slurry onto a porous substrate, the material could be consolidated quickly to create complex structures with local alignment [29]. A promising approach could therefore be to combine DIW with magnetic orientation of liquid slurries with adjusted viscosities and deposited them onto a porous substrate.

In this work, we developed a magnetically assisted direct ink writing method (M-DIW) that continuously printed a liquid slurry with a high concentration in magnetically functionalized microparticles of various chemistry using a porous substrate as the print bed to create microstructured materials for diverse applications. First, the printing strategy is described in detail to highlight the important printing parameters and their theoretical determination. Second, the dynamic alignment of magnetically responsive alumina microplatelets (mAl_2O_3) is studied in background liquids of various viscosities controlled by fumed silica. This allows for a better understanding of the relationship between magnetic alignment and background liquid viscosity. Following, aqueous inks containing 4 wt% of fumed silica with various mAl_2O_3 concentrations are studied to find one that orients with the highest concentration of microplatelets and another one that is printable and orientable. Having determined that the ink containing 20 wt% mAl_2O_3 meets our requirements, microstructured materials are 3D printed continuously and in multilayers. The prints can be turned into ceramics with anisotropic properties, such as flexural strength, magnetic response and self-shaping ability. Finally, to demonstrate that M-DIW is a general method, we use the same strategy to develop an ink containing magnetically responsive graphite microplatelets and print microstructured composites with anisotropic and high electrical conductivity. With M-DIW, we therefore achieve continuous 3D printing ensuring time and cost-efficiency, multimaterial capability, microstructure control with high concentrations of reinforcing elements, and in 3D shapes. This approach opens up many opportunities to fabricate multifunctional materials and devices with tailored and enhanced properties.

2. Materials and methods

2.1. Materials

EMG 605 Ferrofluid (cationic) containing 3.9% vol SPIONs was supplied from Ferrotec Corporation, USA. Graphite was provided by ANR Technologies Pte Ltd. Al_2O_3 microplatelets (lateral size: 5 μm, thickness: 700 nm) were obtained from Kinsei Matec Co., Ltd. Fumed Silica (aerosol 255) was provided by Nippon Aerosil Co., Ltd. Resin (urethane dimethacrylate 55–75 wt%, methacrylate monomer 15–25 wt %) was bought from Formlabs, Inc. Commercial gypsum was purchased from Creativ Company A/S, Denmark. A commercial neodymium magnet (size: 35 $\times$10 x 10 mm) and a DC geared motor were obtained from RS Components Pte Ltd, Singapore.

2.2. Methods

2.2.1. Preparation of magnetically responsive Al_2O_3 (mAl_2O_3)

10 g of Al_2O_3 microplatelets were dispersed into 400 mL of distilled water for 10 min. A controlled volume of Ferrofluid was diluted in 100 mL of distilled water and added to the above suspension drop by drop. The solution was left to stir for 3 days to allow the electrostatic adsorption to occur. After filtering out the water, the microplatelets were washed with water and ethanol before being dried overnight in an oven (IKA OVEN 125) at 48 ℃.

2.2.2. Preparation of magnetically responsive graphite (mGr)

2 g graphite dispersed in 20 mL ethanol was ground by ball milling (Retsch PM 100, milling balls of diameters 5 and 3 mm) at the speed of 500 rpm for 4 h and the intervals of 5 min with 2 min break to decrease their size and generate oxygen groups on their surface. After filtering, the ball-milled graphite microplatelets were redispersed in water to add the diluted ferrofluid dropwise as for the Al_2O_3. The solution was let to stir for 3 days. After filtering out the water, the obtained graphite microplatelets were washed with distilled water and ethanol before being dried in a freeze-dryer (Martin Christ/Alpha 2–4) and subsequently in an oven at 48 ℃.

2.2.3. Determination of the alignment time of magnetized microplatelets as a function of the viscosity

0.1 wt% magnetic platelets (mAl_2O_3 or mGr) were dispersed for 10 min at 2000 rpm in the resin with various content in fumed silica using a mixer (THINKY ARE-250). A drop of the ink was deposited on a glass slide and covered by a small piece of glass and placed under an inverted optical microscope (Nikon EPIPHOT 200). A rotating magnet was placed next to the lens of the microscope at a distance of 1 cm so that the magnetic field strength measured by gaussmeter (HIRST, Magnetic Instruments Ltd) in the drop was 100 mT. The rotating frequency of the magnet was set to 2 Hz and controlled by DC geared motor. Images were captured and analyzed using Image J.

2.2.4. Printable ink preparation

Known amounts of magnetically responsive microplatelets were dispersed in 4 wt% fumed SiO_2 water solution by mixing for 10 min at 2000 rpm in the Thinky mixer followed by magnetic stirring for at least 3

days to make platelets dispersed homogeneously before using in the 3D printer. The amount of mAl_2O_3 added to the 4 wt% fumed SiO_2 solution was varied from 15 wt% to 35 wt%, leading to various vol% in SiO_2 and mAl_2O_3 in the final ink (Table 1).

2.2.5. 3D magnetic printing

The 3D magnetic printing set-up was composed of a commercial 3D Printer (3D Potter Micro 8, 3D Potter Inc. USA) and a magnetic set-up in which a commercial neodymium magnet was fixed on DC geared motor. The defined position of the magnet set-up depends on the orientation intended for the microplatelets in the ink. The magnetic field strength of 100 mT was controlled by placing the magnet at the distance of 1 cm next to the tip of nozzle. For printing, the ink was loaded into syringes of 5 mL (TERUMO SYRINGE, TERUMO CORPORATION) equipped with needles (diameter: 1.2 mm, Nordson EFD) and inserted into the 3D printer. The CAD model was drawn using Rhinoceros 3D and sliced using IdeaMaker. NC Viewer was used to adjust the G code due to the shrinkage during the M-DIW process. The printing speed was fixed at 1 mm/s. The flowrate used was 400%. The printed thickness for each layer was set 0.2 mm. The material was extruded by the motion of the piston of the printer which was controlled by the flowrate. The substrate of porous gypsum was used to quickly jam and dry the ink during the 3D printing process. Gypsum powder of 8 g was dispersed into water of 8 g and subsequently left in oven of 48 °C overnight. The obtained gypsum has total porosity of 60% and density of 1.2 g/ mL.

2.2.6. Sintering and heat treatment

The 3D printed mAl_2O_3 samples were sintered in air for 2 h at 1600 °C in a box furnace (Nabertherm, Switzerland). The heating rate was set at 2.5 °C/min with an intermediate plateau of 5 h at 500 °C. The reduction of the 3D printed mGr composites was conducted at 1050 °C for 4 h with a heating rate of 5 °C/min in a tube furnace within an Argon atmosphere (Protege XST split tube furnace).

2.3. Materials characterization

The rheological properties of the inks were measured by using a rheometer (Bohlin, Malvern Instruments) using 15 mm serrated plates with a gap of 500 μm and at room temperature. Amplitude sweeps were carried out from 0.1 Pa to 1000 Pa using oscillation mode at the frequency of 1 Hz. The Viscometry mode measurements were carried out for shear rates from 0.001 s^{-1} to 100 s^{-1}. All measurements were repeated at least three times.

Zeta potential measurements were conducted on the surface charge of particles using dynamic light scattering (Horiba SZ-100). The ink was diluted 10 times and slowly loaded into the electrode cell for the measurement. Every sample was tested three times.

Electron microscopy was carried out after the sample was coated with 10 nm gold and observed using a SEM (JSM-7600 F and JSM-5600 LV, JEOL, Japan). Printed green body was cryogenically fractured using liquid nitrogen and ceramics was polished using SiC paper before coating gold.

The anisotropic shrinkage was measured on horizontally and vertically aligned samples after sintering up to the temperature of 1600 °C with the heat rate of 5 °C/min in TA Instruments' optical dilatometer, ODP 868. The measurements were averaged over 3 samples.

The phase composition of the sintered ceramic composite was evaluated by X-ray diffraction (XRD; PANalytical EMPYREAN, The Netherlands) using Cu Kα radiation with operation at 30 kV and 20 mA.

The hardness was measured using a Vicker's indenter (Future-Tech microhardness tester FM-300E) at a loading force of 2000 g and dwell time of 10 s. Prior to the test, the samples were embedded in an epoxy resin (MS-1000) and mechanically polished using a combination of SiC paper and colloidal silica suspension (OP-U, 1 and 0.3 μm, Struers, Denmark). Ten indents were made for each sample. The indented areas were observed under optical microscopy.

Flexural strength and modulus values were obtained using 3-point bending in a Shimadzu AGS-X mechanical testing machine equipped with a 10 kN load cell. The span of the three-point bending jig was 15 mm. The size of the tested sample was 20 × 3.5 × 0.4 mm^3. The measurements were carried out by monotonically loading the specimens at a constant displacement rate of 1 mm min^{-1}. At least 5 specimens were tested for each composition.

Electrical conductivity was measured by four-point probe approaches equipped with multi digital meter (Agilent 34401 A 61/2 Digit Mulitmeter).

The densities of samples were determined using Archimedes' as the following formula:

$$\rho = \rho_w \mathbf{x} \frac{W_A}{W_{IA} - W_{IW}}.$$

where ρ is the density of the ceramic composites, ρ_w is the density of water, W_A is the dried weight,W_{IA} and W_{IW} are the weight of the impregnated sample measured in air and water, respectively.

3. Results and discussion

3.1. 3D printing and ink design strategy

To achieve continuous 3D printing using DIW, while orienting 2D microplatelets with an external magnetic field, the ink and the printing process should be appropriately designed (Fig. 1). First, the ink should contain magnetically responsive particles that biaxially align when a low magnetic field is applied. Second, the ink should be extrudable through a thin nozzle. Third, the ink should solidify in a short time to permit multilayer printing, while still allowing enough time for the magnetic orientation of the microplatelets suspended in the ink. The ink should therefore satisfy antagonistic requirements: it should be viscous enough to be extrudable and buildable (i.e., printable), while being liquid enough to allow the microplatelets to align with the magnetic field. The strategy proposed to realize those antagonistic requirements is described in the following.

Magnetically responsive microplatelets are obtained by coating them with superparamagnetic iron oxide nanoparticles (SPIONs) of 10 nm diameter using electrostatic interactions by choosing SPIONs with a surface charge opposite to that of the microplatelets (Fig. 1A) [2]. The simplicity of this functionalization approach will grant our 3D printing the capability to print a large range of materials since a large variety of

Table 1
Detailed composition of the inks containing the percentage of Al_2O_3, SiO_2 and Fe_3O_4.

Name	Initial SiO_2 wt% solution	wt% of mAl_2O_3 added to the SiO_2 solution	vol% of SPIONS with respect to Al_2O_3	Total vol% in the ink of:		
				SiO_2	mAl_2O_3	Fe_3O_4
15 wt% mAl_2O_3	4	15	14	1.5	3.7	0.5
20 wt% mAl_2O_3	4	20	14	1.5	5.2	0.7
25 wt% mAl_2O_3	4	25	14	1.4	6.8	0.9
28 wt% mAl_2O_3	4	28	14	1.4	7.8	1.1
30 wt% mAl_2O_3	4	30	14	1.4	8.5	1.2
32 wt% mAl_2O_3	4	32	14	1.4	9.3	1.3
35 wt% mAl_2O_3	4	35	14	1.4	10.4	1.4

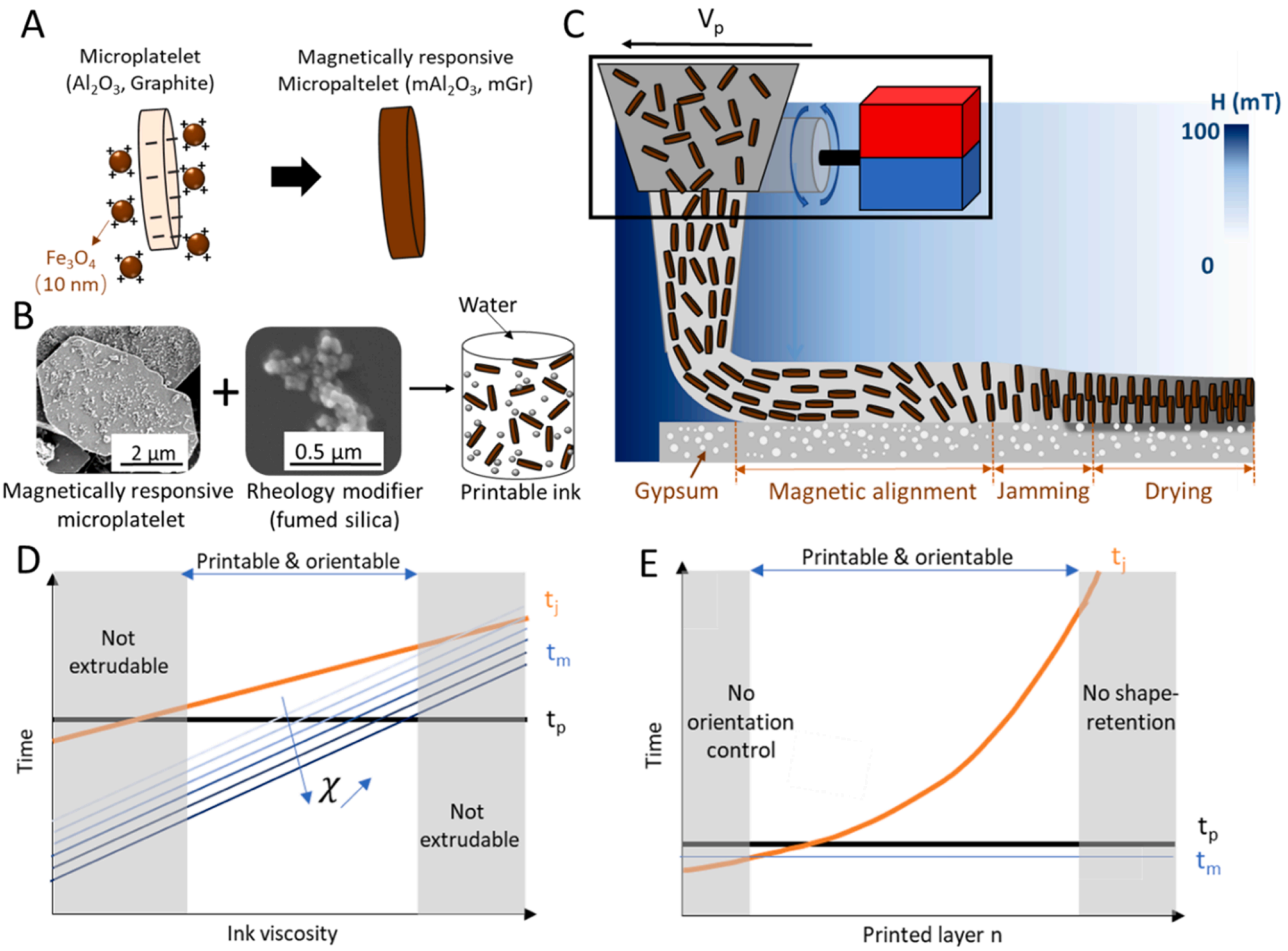

Fig. 1. M-DIW strategy. (A) Illustration of the synthesis of magnetically responsive microplatelets using electrostatic adsorption of Fe_3O_4 superparamagnetic nanoparticles (SPIONs) of 10 nm diameter. (B) The printable ink comprises the magnetically responsive microplatelets and fumed silica as a rheological modifier suspended in water. (C) Schematic of M-DIW: the ink is extruded through a nozzle and deposited onto a porous substrate while a rotating magnetic field is applied. The rotating magnet is attached to the nozzle, and both are moving at a speed V_p. The strength distribution of the magnetic field H is shown by the graded blue color.Microstructure control in M-DIW occurs in three steps: (1) in the freshly deposited ink, the microplatelets present align under the magnetic field; (2) the water from the deposited ink is removed through the porous substrate leading to the jamming of the particles and shape-retention; (3) final consolidation of the layer by drying. (D) Schematic representation of the time for magnetic alignment t_m, time for jamming t_j and time related to the 3D printing t_p as a function of the viscosity. χ is the magnetic susceptibility of the microplatelets indicating a decrease in t_m with increasing χ. The grey areas highlight ink viscosities where the ink cannot be extruded. (E) Schematic representation of t_m, t_j, and t_p as a function of the printed layer number n. The grey areas highlight layers with no orientation control or shape retention.

microplatelets can be functionalized this way, including metallic flakes [30], carbon-based materials [31], BN microplatelets [1], and others. The method can also be used to functionalize microfibers [32]. In this work, we focus on microplatelets as they are generally more challenging to orient in 3D printing. The amount of SPIONs can be tuned depending on the dimensions and other intrinsic properties of the microplatelets chosen. In this work, alumina and graphite microplatelets of diameters 1–10 µm are used to demonstrate M-DIW. The negative surface charges of alumina and graphite enable the absorption of cationic SPIONs (see Supplementary Information (SI) Fig S1 for Zeta Potential measurements), conferring them magnetic response. Rotating magnetic fields can then be applied to align the microplatelets biaxially in the plane of the magnet, when the frequency of rotation of the magnetic field is sufficiently high [33]. This biaxial alignment results from a balance between the viscous and the magnetic torques, which makes it energetically more favorable for the microplatelets to be aligned within the plane of rotation of the magnetic field above a certain frequency than to rotate synchronously with the field.

To obtain the printable ink, the magnetically responsive microplatelets were suspended in water with a rheological modifier. In this study, we used fumed silica as the rheological modifier, which is a commonly used strategy in DIW (Fig. 1B) [34]. Also, the use of a mineral-based additive is interesting in view of printing ceramic materials, where it can form a mineral matrix bonding the microplatelets after sintering. This rheological modifier is required to enable the extrudability and printability of the ink. Indeed, for conventional DIW, the ink should be a paste with high viscosity and elasticity [35]. Without the rheological modifier, the inks composed of microplatelets are either too liquid at low microplatelet concentrations to be printable, or too viscous and brittle at high microplatelet concentrations [23]. The concentrations of microplatelets and fumed silica in the ink therefore have to be balanced to obtain an ink that is viscous enough to be printable, but not too viscous so that the microplatelets can rotate and align with the magnetic field. Our strategy to do so is to find an ink composition where the zero-shear viscosity is high, but the yield stress is low. The high zero-shear viscosity enables extrusion through a thin nozzle without developing severe die swell. Also, it ensures a homogeneous ink without sedimentation. The low yield stress enables the motion of microplatelets under the action of the magnetic torque and their magnetic orientation. Although such ink is extrudable, it is not buildable as the low yield stress

will makes it flowable. Therefore, it will not show shape-retention and no ability to withstand the weight of multiple layers. We address this problem by removing the low viscosity solvent, water, from the ink in a controlled fashion during the printing. Inspired by magnetically assisted slip casting where an aqueous slurry containing magnetically responsive microplatelets is cast onto a porous substrate [36], the removal of water is achieved here by printing onto a porous substrate made of gypsum that removes water by capillary suction (See SI Fig. S2 for the microstructure of gypsum). After water is removed, the microplatelets accumulate at the surface of the gypsum forming a percolated layer. Overall, we therefore, augmented an extrusion-based 3D printer with a porous substrate and a rotating magnet positioned close to the extruding nozzle (see SI Fig. S3 for the picture of the printing set-up). The position and orientation of the magnet can be adjusted to tune the magnetic field strength and alignment direction as desired.

Having described the strategy, M-DIW consists therefore in three steps (Fig. 1C). First, the ink extruded from the nozzle is deposited on the porous substrate while the magnetically responsive microplatelets align the microplatelets with the magnetic field. The rotating magnet and the extruding nozzle move at a speed V_p corresponding to the printing speed. Second, the water from the deposited ink is removed by capillary forces through the substrate, leading to an increase in the viscosity of the deposited ink and the jamming of the microplatelets in their orientation set by the magnet. Third, the jammed deposited layer is further dried by the substrate to strengthen the assembly and allow subsequent layers to be deposited following the same process. For the subsequent layers, the underlying layer acts as the substrate and removes the water by capillary forces.

To effectively control the local microplatelet alignment in the deposited ink, the ink should fulfill antagonistic requirements in terms of viscosity as discussed before. At low viscosities, back-pressure prevents continuous extrusion, whereas at high viscosities, the forces required to extrude become too high for the equipment. In addition, for the alignment of the microplatelets during M-DIW, the following temporal relationships should be fulfilled:

$$\left\{ \begin{array}{l} t_m < t_p \\ t_m < t_j \end{array} \right\}, \tag{1}$$

where t_m is the time required for the magnetic alignment of the microplatelets, t_p a time related to the printing speed ad t_j the jamming time of the ink (Fig. 1D). The timet_p is the time at which the magnetic field where the ink is just deposited is sufficiently strong to orient the microplatelets. Indeed, the magnet is moving with the nozzle. Therefore, the magnetic field in the deposited ink decreases as the nozzle moves away at a speed V_p. The timet_p is thus defined as follows:

$$t_p = \frac{\Delta l}{V_p}, \tag{2}$$

where Δl is the distance traveled by the nozzle where the magnetic field is high enough to align the microplatelets in the deposited ink. The magnetic field strength distribution is set by the magnet used. Here, we used a permanent Neodymium magnet of dimensions 35 × 10 x 10 mm^3. In an ideal scenario, a high printing speed is desired, therefore a low t_p. This poses constraints on t_m as the magnetic field at one point in the deposited ink should be high enough for the microplatelets to align quickly. The time t_m is given by:

$$t_m = \frac{6\pi^2 V \frac{f}{f_0} \eta_0}{\frac{4\pi\mu_0\chi^2}{3(\chi+1)}\left[(a+d)(b+d)^2 - ab^2\right]}, \tag{3}$$

where V is the volume of a microplatelet, $\frac{f}{f_0}$ the Perrin friction factor, η_0 the viscosity of fluid, μ_0 the permittivity of vacuum, a and b the average thickness and diameter of the microplatelet, respectively, d the thickness of the magnetic coating, and χ the magnetic susceptibility of the microplatelets [27]. For a given ink composition, t_m is proportional to $\frac{\eta_0}{\chi}$ according to Eq. (3). An easy way to decrease t_m and ensure $t_m < t_p$ is therefore to increase χ by increasing the magnetic coating of the microplatelets. Furthermore, the jamming time t_j after the ink is deposited onto the printed substrate is given by:

$$t_j = \frac{\eta_0 R}{2J\Delta P} x^2 \tag{4}$$

where R is the hydrostatic resistance, J the ratio between the volume of the consolidated layer and of the extracted liquid, ΔP the capillary suction and x the distance to the substrate [5]. t_j therefore, increases with η_0. In general, suspensions of particles have a long t_j as compared to t_m [28]. However, Eq. 4 indicates that the first printed layers (small x and high ΔP) have a very short jamming time and likely cannot achieve $t_m < t_j$. Indeed, the strong hydrodynamic forces that develop at the surface of the porous substrate inevitably lead to horizontally aligned structures [28]. Also, t_j increases with x and therefore increases with the number of layers n (Fig. 1E). A too long t_j would require setting a lower V_p as the layers need more time to jam before the next layer can be deposited. Also, a too long t_j may not be able to maintain the shape retention when 3D printing the next layers. To decrease t_j and realize a high number of layers in the print, other solvent removal methods can be used, such as external heat [23].

To realize our M-DIW printing strategy, we highlighted the importance of the viscosity of the ink and the relationships between three critical times. In the next section, we use Al_2O_3 microplatelets to demonstrate M-DIW. We first focus on understanding the relationship between η_0 andt_m for single mAl_2O_3 microplatelets. This will help us design inks that are extrudable, yet where magnetic alignment can occur with a low t_m.

3.2. Alignment dynamics of single microplatelets

In this section, magnetized alumina microplatelets (mAl_2O_3) of average diameter 5 μm were suspended at various concentrations in background fluids of viscosities η_0. The times t_m taken for the microplatelets to align with a magnetic field of 100 mT were measured. The magnetic susceptibility χ of the microplatelets was also varied to reduce t_m (Fig. 2).

Although the M-DIW strategy comprised a solvent that was removed during printing, in this set of experiment, a resin was used instead of the solvent. The reason for using a resin instead of the fumed silica suspension was to be able to span a large range of viscosities, whereas with the fumed silica, a small increase in concentration led to 2 orders of magnitude increase (for instance, 12–13 wt% of fumed silica in water led to a viscosity increase from 20 to 1000 Pa·s). Furthermore, the resin prevented the formation of aggregates and a homogeneous dispersion of the particles, whereas the absence of an evaporating liquid permitted to ensure no drying during the experiment. The resin was a liquid epoxy with low zero-shear viscosity η_0 of around 20 Pa·s. The addition of 5–8 wt% SiO_2 to the resin increased η_0 from 30 to 700 Pa·s and its yield stress σ_y from 0 to 45 Pa (Fig. 2A and B). At the same time, the elastic and viscous moduli G' and G'' increased by two orders of magnitude and the shear-thinning and thixotropic properties required for traditional DIW were obtained with 8 wt% SiO_2 (see SI Fig. S4 for the oscillatory rheology data and Herschel-Bulkley fits).

The Al_2O_3 microplatelets were coated with SPIONs up to a maximum of 18.6 vol% with respect to the microplatelets (see SI Table S1 for the corresponding χ). To measure t_m, we used an inverted optical microscope to observe the dynamic response of the mAl_2O_3 when subjected to a magnetic field of 100 mT rotating at a frequency of 2 Hz. The alignment degree D_L/D_W was determined by taking the ratios of the long and short diameters at the full width of half-maximum of Lorentz fits, respectively, of the ellipse of the Fast Fourier Transforms (FFT) of the microscopic images (see SI Fig. S5 for details). A $D_L/D_W = 1$ indicates no

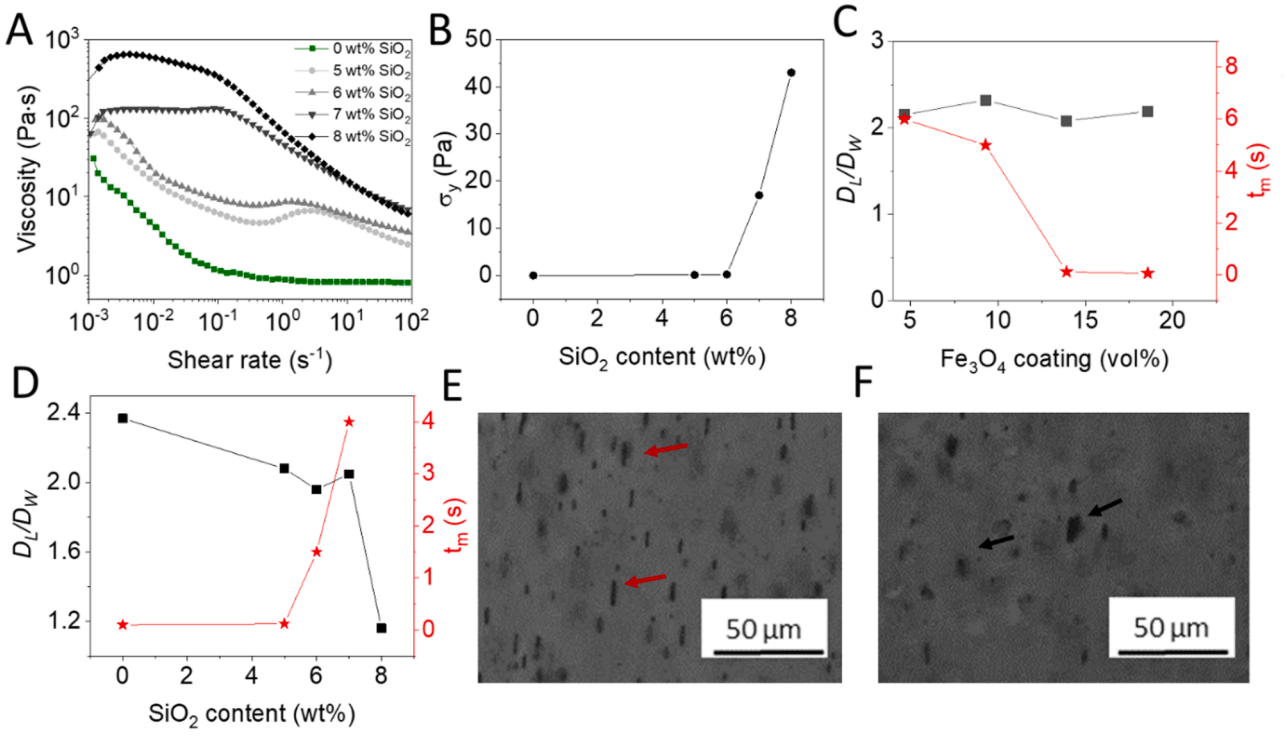

Fig. 2. Alignment dynamics of mAl_2O_3 microplatelets under rotating magnetic fields of 100 mT. (A) Viscosity as a function of the shear rate for the resin with varying wt% of fumed silica. (B) The effect of varying wt% of SiO_2 on the yield stressσ_y of the ink. (C) Alignment degree D_L/D_W (black) and time for alignment t_m (red) as a function of the Fe_3O_4 coating, in the resin with 5 wt% SiO_2. (D) D_L/D_W (black) and t_m (red) of the microplatelets with 14 vol% Fe_3O_4 coating as a function of the wt% of SiO_2 in the resin. (E) Optical micrograph showing the microplatelets with 14 vol% SPIONs biaxially aligned in the resin with 7 wt% SiO_2. The red arrow points to a microplatelet. (F) Optical micrograph showing that alignment is not achieved for the microplatelets with 14 vol% SPIONs, suspended in the resin containing 8 wt% SiO_2. The black arrows point to misaligned microplatelets.

alignment, whereas $D_L/D_W > 1$ indicates magnetic alignment. As expected from Eq. 3, increasing the amount of SPIONs on the microplatelets increased their magnetic response and resulted in a shorter alignment time t_m. In both the pure resin (see SI Fig. S6) and the resin with 5 wt% SiO_2 (Fig. 2C), t_m decreased from 6 to 0.1 s by increasing the SPIONs coating from 5 to 18 vol% while maintaining a high alignment quality with a $D_L/D_W > 2$. However, t_m increased with the SiO_2 content (Fig. 2D). In the resin with 7 wt% SiO_2, alignment could still take place, with a t_m of 4 s (Fig. 2E). In the resin with 8 wt% SiO_2, no alignment occurred (Fig. 2F). Even with 18 vol% coating, the resin containing 8 wt % SiO_2 did not allow for the magnetic alignment. This study of the influence of the background liquid on the magnetic orientation of the microplatelets therefore indicates that mAl_2O_3 can align with low magnetic fields when the yield stress of the liquid is $\sigma_y <$ 45 Pa.

Furthermore, we found that mAl_2O_3 microplatelets with a SPIONs coating of 14 vol% aligned with a t_m of 4 s only when suspended in background liquids of viscosities at zero shear less than 100 Pa.s and with a yield stress < 45 Pa. Since it is preferable to use a minimum amount of SPIONs, we used 14 vol% in the subsequent experiments. To prepare a M-DIW ink containing a high concentration of microplatelets for enhanced properties in the final printed part, we therefore need to ensure that $\sigma_y <$ 45 Pa for this ink. Now the rheological properties of the ink and not of the background liquid have to be considered as the microplatelets will start interacting, thereby augmenting the ink viscosity. In the following, the background liquid in the ink was thus chosen to be water with 4 wt% of fumed silica. This background is very liquid and individual microplatelets can easily align. A SPIONs coating of 14 vol% for the mAl_2O_3 is chosen given the considerations discussed above. The concentration of mAl_2O_3 in the ink is then varied to find the maximum concentration where 3D printing, and magnetic orientation can be achieved simultaneously.

3.3. Ink optimization for M-DIW

To develop a printable and orientable ink containing a high concentration of mAl_2O_3 microplatelets, we hypothesized that the magnetic orientation of individual microplatelets depends on the yield stress of the ink and varied the concentration of mAl_2O_3 (Fig. 3). Achieving a high microplatelet content in 3D printed parts with local biaxial orientation is so far not possible with current technologies and is expected to enhance the properties of the part while having a large design space of microstructural design.

To find the ink with the highest loading in mAl_2O_3 while having magnetic alignment, the mAl_2O_3 with 14 vol% SPIONs coating was dispersed in an aqueous solution containing 4 wt% SiO_2 and the content in mAl_2O_3 was increased from 15 up to 35 wt%, which correspond to 4.1–11.6 vol% of mAl_2O_3. The viscosity at zero shear of the inks increased from 10 Pa·s for 15 wt% loading of microplatelets to 3000 Pa·s for 35 wt% (Fig. 3A). All inks exhibit shear-thinning behavior (Fig. 3A) and their yield stress increases from 4 Pa for the ink containing 20 wt% mAl_2O_3 to 45 Pa for 35 wt% concentration (Figs. 3B and S7A). Additionally, the inks containing more than 15 wt% microplatelets present a solid-like behavior (G' > G'') at low shear rates (Fig. S7B). This suggests that some shape-retention can be obtained for these inks. In turn, the inks containing 0 and 15 wt% mAl_2O_3 exhibit liquid-like behavior (G' ≈ G''), indicating no strong interaction between SiO_2 nanoparticles and mAl_2O_3 microplatelets (Figs. S7B and S8B). These results reveal the formation of a percolating network structure in the ink starting at 20 wt% mAl_2O_3 [37]. Based on our results in the previous section, it is expected that magnetic alignment will be possible for all inks with the yield stress lower than 45 Pa, except for 35 wt% concentration. At 35 wt%, the high yield stress indicates that the microplatelets strongly interact with each other, preventing their orientation with the low magnetic field as used here.

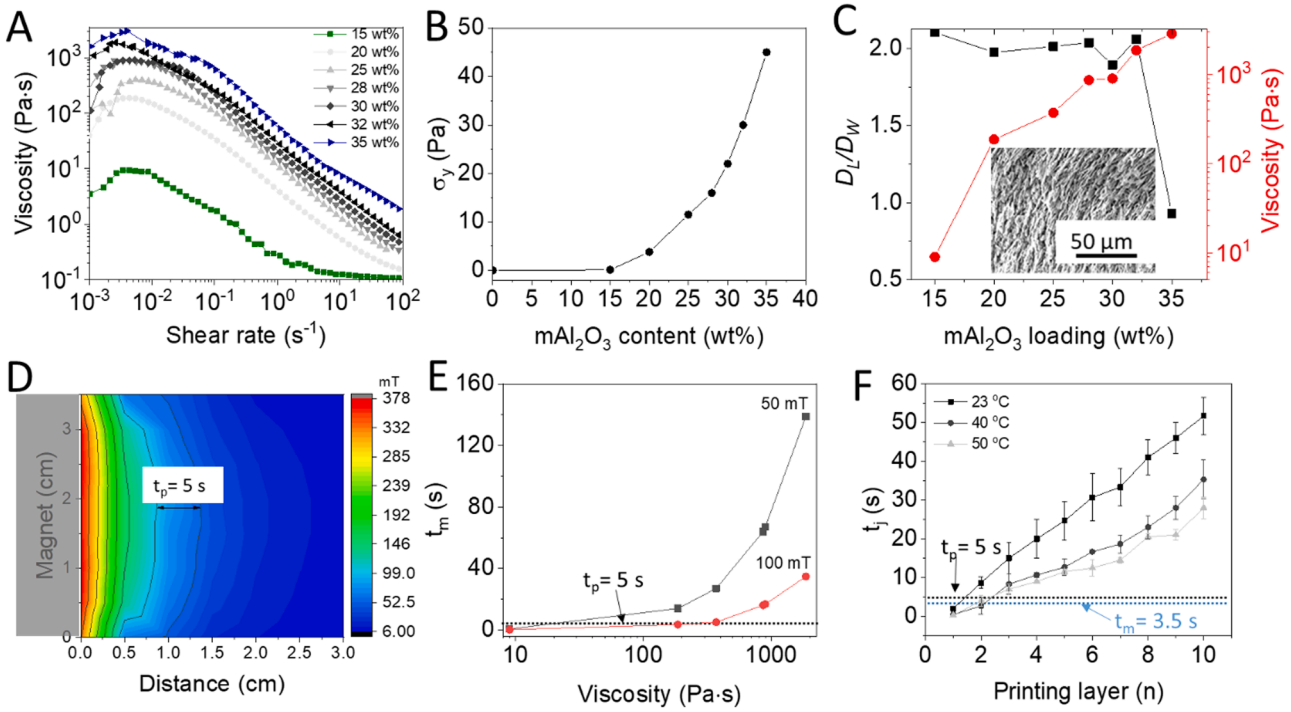

Fig. 3. Ink optimization for M-DIW using mAl_2O_3 microplatelets coated with 14 vol% SPIONs. (A) Viscosity as a function of the shear rate for aqueous inks containing 4 wt% SiO_2 and increasing concentrations in mAl_2O_3 microplatelets. (B) The effect of varying wt% of mAl_2O_3 on the yield stressσ_y of inks containing water and 4 wt% SiO_2. (C) Alignment quality D_L/D_W (black) and zero-shear viscosity of the ink (red) as a function of the microplatelet loading. The insert is an electron micrograph showing vertical alignment in the ink containing 32 wt% mAl_2O_3 microplatelets, obtained by slip casting on gypsum. (D) Spatial distribution of the magnetic field generated by the permanent magnet at the nozzle. For a printing speed V_p set at 1 mm/s, it takes $t_p = 5$ s for the deposited ink to see the magnetic field decrease from 100 mT to 50 mT as it gets printed. (E) Theoretical calculation of t_m as a function of the viscosity of the inks, for a magnetic field of 50 and 100 mT. (F) Jamming time t_j as a function of the printed layer number n when printing on gypsum at 23, 40, and 50 °C, for the ink containing 20 wt% mAl_2O_3.

To verify that magnetic alignment occurs as predicted, we measured the ratio D_L/D_W from electron micrographs instead of optical images (Fig. 3C). The direction of alignment was set to orient the microplatelets vertically with respect to the horizontal substrate. This orientation was chosen since it is the least favorable to obtain as gravitational forces and hydrodynamic forces due to the capillary suction need to be overcome. The inks were manually deposited onto the porous substrate, oriented vertically, and left to dry. As predicted, all inks could be aligned except the ink with 35 wt% microplatelets (see insert in Fig. 3C).

To determine which of these inks can be 3D printed,t_m,t_j and t_p need to be assessed as discussed previously. In our printing set-up, the magnet is fixed on a motor and moves along with the dispensing nozzle. For this magnet, the magnetic field strength varies in space from 378 mT at the surface of the magnet to 6 mT at a distance of 3 cm (Fig. 3D). To avoid the magnet to hit the nozzle while rotating, it was placed further away so that the field strength at the nozzle tip is 100 mT. Continuously 3D printing at a constant speed V_p of 1 mm/s, the magnetic field applied to the deposited ink gradually decreases from 100 mT to 50 mT in 5 s. This printing speed is reasonable for 3D printing. Therefore, t_p is set at 5 s and we need to ensure $t_m < 5s$. Faster printing speed to improve the printing efficiency can be possibly achieved by applying wider spatial distribution of magnetic field strength above 50 mT, for example using a magnet with a different geometry.

Since the high concentration of mAl_2O_3 in the ink makes it difficult to see the individual platelets under an optical microscope, thet_m therefore were calculated using Eq. (3), for magnetic field strength of 100 mT and 50 mT (Fig. 3E). When considering low concentrations of microplatelets dispersed in fluids of various viscosities previously, we used the viscosity of the liquid background as η_0 in Eq. (3). Now that the concentration of microplatelets is high, they are susceptible to interact and to hinder each other rotation, therefore it is the viscosity of the ink, i.e., the background liquid and the other microplatelets, that is taken as η_0 in Eq. (3). The prediction shows that the mAl_2O_3 microplatelets can be aligned in inks of viscosities 2000 Pa.s within 40 s for a magnetic field strength of 100 mT and 140 s for 50 mT. In practice, the calculated plot was used to find the ink viscosity required to obtain a $t_m < t_p = 5$ s. At 100 mT, inks of viscosities up to 400 Pa.s can be aligned. This corresponds to inks containing 20–25 wt% mAl_2O_3. This means that the inks containing as much as 20 wt% mAl_2O_3 can be aligned during M-DIW.

The ink containing 20 wt% mAl_2O_3 exhibited a 5 Pa and thus the water removal through the porous substrate was crucial to ensure shape retention. t_j was therefore measured for this ink as a function of the number of layers printed (Fig. 3F). At 23 °C, t_j increased with the number of layers, as expected from Eq. (4) (see SI Fig. S9 for the casting kinetics). Indeed, as more layers are deposited and the thickness of the print increases, the removal of the water slows due to the increased tortuosity. The first layer had $t_j < 2s < t_m$ and therefore no alignment control can be obtained in the first layer, which corresponds to the experimental results (see SI Fig. S10 for an electron micrograph of the first layer). After 10 layers, $t_j \sim 1$ min which makes it challenging for printing thicker parts. To increase the number of layers, t_j could be reduced by half by adding heat to the substrate. Therefore, a compromise must be made between obtaining controllable alignment in the first layers and being able to print a large number of layers.

To demonstrate that microstructural control in the 3D printed part is effective, we used the ink containing 20 wt% mAl_2O_3 and adjusted the direction of the rotating magnetic field during printing (Fig. 4). In printed layers above the first layer, horizontally aligned microplatelets and vertically aligned microplatelets with their basal plane perpendicular or parallel to the printing direction can be realized (Fig. 4A). The quality of the alignment was similar to what was obtained without the 3D printing, with a D_L/D_W of 1.9. Since the microstructure depends on the external magnetic field, any microplatelet 3D orientation can be

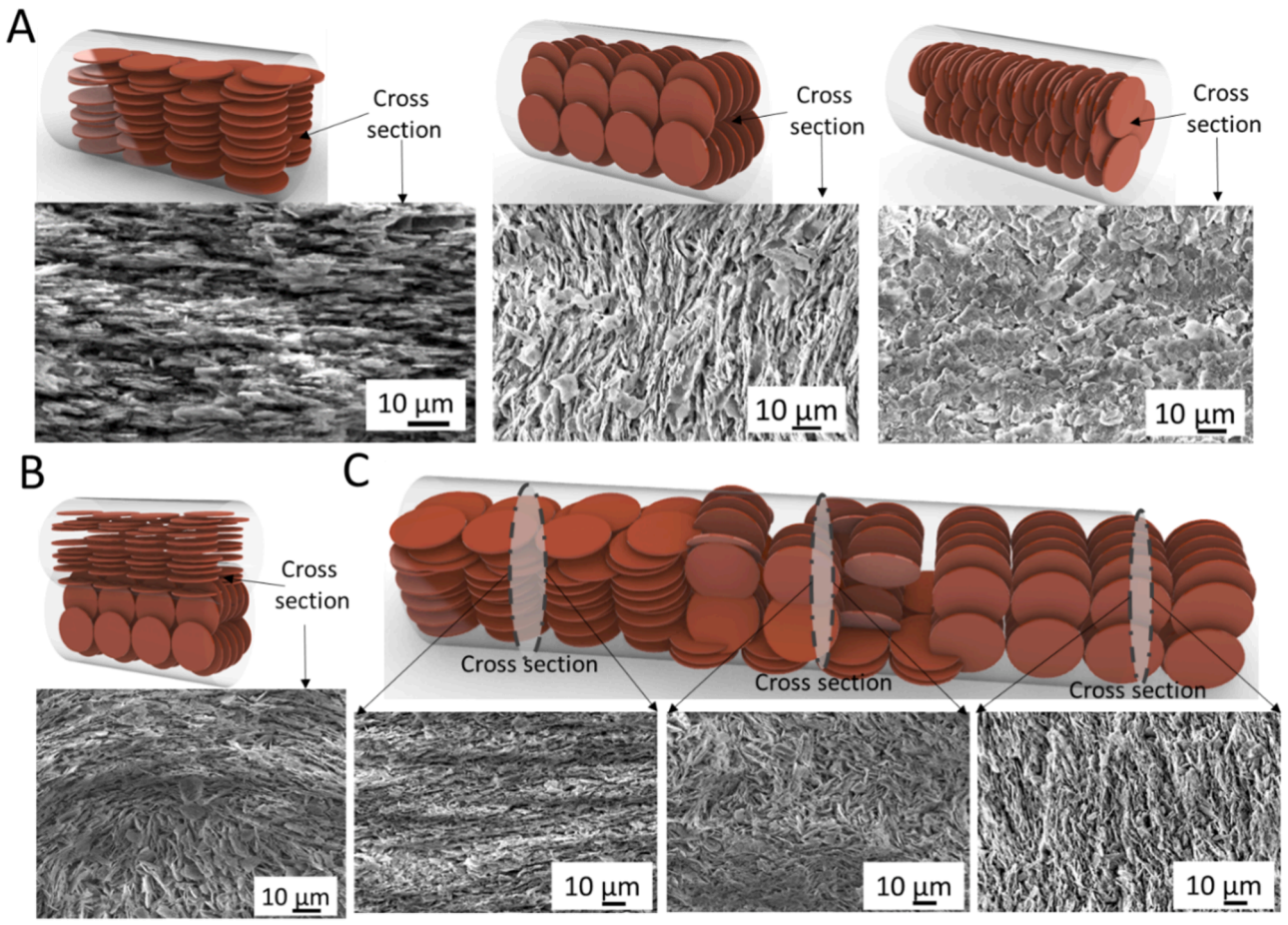

Fig. 4. 3D printed microstructures obtained with the aqueous ink containing 20 wt% mAl_2O_3 in 4 wt% SiO_2 (A) Schematics and corresponding electron micrographs showing horizontal alignment (left) and vertical alignment with the basal plane of the microplatelets perpendicular to the printing direction (middle) and parallel to the printing direction (right). (B) Schematics and corresponding electron micrograph showing the two different alignments in two consecutive layers. (C) Schematics and corresponding electron micrographs showing that a single printed line with horizontal and vertical alignment.

achieved. Although the current M-DIW set-up has a magnet fixed to a motor and attached to the nozzle, a more advanced version of the set-up could include a magnet whose rotation angle is programmed remotely. The magnetic control could also be included into the CAD file that is loaded into the 3D printer. Although we did not have such automation yet, we could nevertheless change the magnetic orientation manually to demonstrate that local orientation can be obtained in the printed parts, between layers (Fig. 4B) as well as within a single layer (Fig. 4C). Some lightly misaligned segments of about 100 μm could be observed between well-aligned regions. These misaligned domains are attributed to the manual change in orientation of the magnet. Therefore, the ink containing 20 wt% mAl_2O_3 is a good ink for M-DIW. Interestingly, we found that the ink containing 15 wt% mAl_2O_3 could also be printed despite the very low viscosity at zero shear of about 10 Pa.s.

Having established how to obtain a printable ink for DIW with controlled local magnetic orientation, we next demonstrate the advantage of having these capabilities by printing ceramics and composite materials with controllable properties using the ink containing 20 wt% mAl_2O_3.

3.4. Properties of microstructured ceramics obtained using M-DIW

Being able to 3D print a colloidal solution containing oriented microplatelets is interesting for multiple reasons. First, the printed material is an assembly of inorganic particles at high solid loading. For our printable and orientable ink, the relative density measured after printing was about 31%. In the solid part, the concentration of microplatelets is very high of 70 vol%, the rest being made of 20 vol% SiO_2 and 10 vol% Fe_3O_4. In the final printed body, there was thus about 22 vol% microplatelets. Such concentration of oriented anisotropic microplatelets could not be realized in other 3D printing methods which typically achieve only 15 and 4.7 vol% [20,27]. A high concentration of inorganics can lead to highly reinforced composites after their infiltration with a polymer or can be turned into ceramics after sintering. Therefore, our strategy can be adopted on a wide range of products. Secondly, the control of the microstructure allows local properties for multifunctional parts. For example, one section could be printed with vertically oriented microplatelets to increase the hardness and the wear resistance, whereas another region could have horizontally oriented microplatelets to have higher strength. In the following, we present some of the properties that can be obtained in microstructured ceramics using the ink containing 20 wt% alumina in 4 wt% fumed silica (Fig. 5).

Using this ink, 3D shapes, porous lattices, and bulk samples were 3D printed (Figs. 5A and S11). The resolution of the layer height was 0.1 ± 0.02 mm and the line width was 1.2 ± 0.3 mm. Up to 30 layers could be deposited, leading to samples of about 3 mm thickness. Although no overhangs could be obtained because of the drying approach, we can envision printing a sacrificial material to create them. Here, we turned the printed parts into ceramics by sintering at 1600 °C. The high temperature treatment maintained the iron oxide (Fe_3O_4) in ceramic (see SI Fig. S12 for the XRD data of the sintered ceramic), which possessed magnetic properties and could be easily attracted to a magnet. This is an interesting property for making actuated structures. For example, the sintered ceramics can later be combined with a soft polymeric matrix to

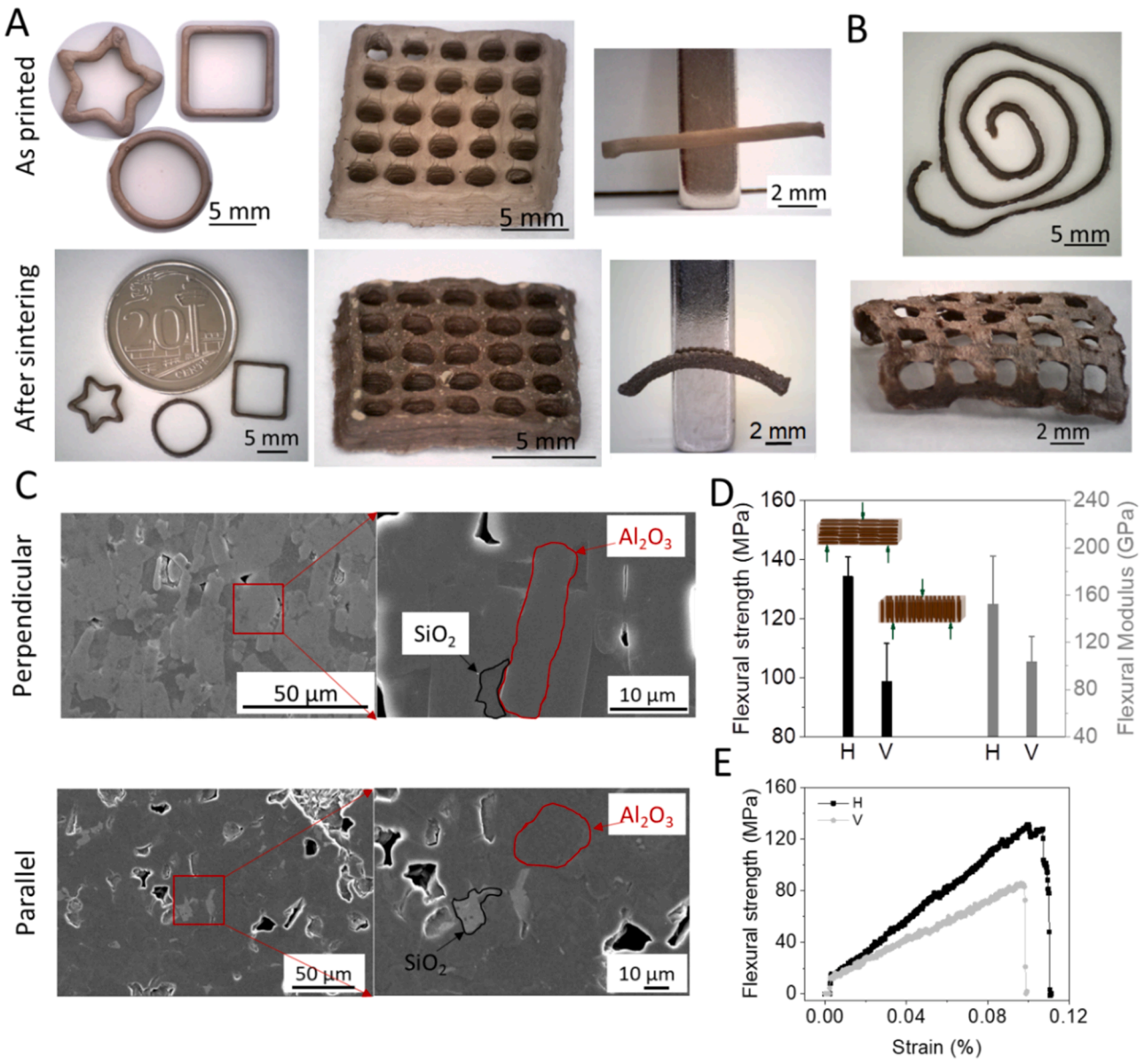

Fig. 5. Microstructured alumina ceramics obtained using M-DIW. (A) Images of 3D printed samples as printed and after sintering: 3D shapes made of 10 layers (left), lattice structure made of 30 layers (middle) and bulk sample made of 10 layers which has been attracted to a magnet. (B) Complex 3D structures obtained after self-shaping during the sintering process. (C) Electron micrographs showing the microstructure of the sintered ceramics with vertically oriented grains. The cross-sections were taken perpendicular (top) and parallel (bottom) to the basal plane of the grains. (D) Flexural strengths (black) and flexural moduli (grey) for horizontally aligned (H) and vertically aligned (V) sintered specimens. (E) Representative flexural stress–strain curves of printed ceramics with horizontal (H, black) and vertical (V, grey) orientations, respectively.

create a magnetically actuated gripper (see SI Fig. S13 for a demonstrator).

Furthermore, the shape of samples with a unique orientation was maintained with a good resolution after the sintering without deformation. On the contrary, samples with a bilayer microstructure, such as with horizontal layers and vertical layers morphed because of the anisotropic shrinkage between the two layers. This morphing ability could be used to fabricate ceramics with unusual shapes that could not be made otherwise. Self-shaping ceramics have been reported in the literature, but the ability to 3D print them provides a larger range of structures and a greater design space.[38] Herein we designed a coil by printing a shape with 2 layers containing horizontally aligned microplatelets and 8 layers with vertically aligned microplatelets (Fig. 5B). A curved lattice structure could also be obtained after sintering of lattice structure with 3 layers with horizontal alignment and 3 layers with vertical alignment. Our ceramics could deform to a much greater extent than that was reported in the literature on self-shaping ceramics thanks to the thin dimensions of our prints and the large shrinkage anisotropy. Indeed, after sintering, the shrinkage of the printed ink with 20 wt% mAl_2O_3 perpendicular to the basal plane of the microplatelets was of $39.4 \pm 1\%$, whereas the shrinkage parallel to the basal plane was $22.3 \pm 2.9\%$ (see SI Fig. S14 for the shrinkage data). This high shrinkage is attributed to the densification of ceramic and the melting of the fumed silica during the sintering.

Furthermore, the sintered ceramics had a density of 3 g/cm^3 with total porosity of 23% and retained their microstructure after sintering (Fig. 5C). This demonstrates the good capability to 3D print bioinspired ceramics such as nacre-like alumina [39,40]. Our 3D printed nacre-like ceramics exhibited a hardness of 7.86 ±1.12 GPa on vertically-oriented microplatelets and 7.38± 1.06 GPa on horizontally-oriented

microplatelets (see SI Fig. S15). The slight difference of hardness despite the anisotropic microstructure is likely due to the remaining porosity and glassy interfaces. Yet, the ceramics exhibited anisotropic flexural properties with a flexural strength of the horizontally aligned ceramics 36% higher than the vertically aligned ones, reaching a value of 134±6.5 MPa (Fig. 5D and E). Likewise, the flexural modulus of the horizontally aligned samples was 50% higher than the vertically aligned ones, reaching a value of 152 ± 40 GPa (Fig. 5E). These good mechanical properties resulted from the densification, the well-aligned microstructures, as well as the strong interface between the alumina grains and the silica matrix. Indeed, element mapping showed that Fe and Si diffused in Al_2O_3 during sintering (see SI Fig. S16). Compared to other nano-silica-reinforced alumina ceramics obtained by a 3D printing method, our ceramics had a bending strength about 3 times higher [41]. Compared to other microstructured alumina obtained by DIW by Feilden et al., the flexural properties are similar but we can control the orientation as desired [18]. High density alumina ceramics have been obtained using 3D printing, for example via vat photopolymerization and digital light processing [42,43]. Although the ceramics obtained were dense and had a flexural strength > 450 MPa, microstructural control was not feasible limiting the possibility of design [44].

M-DIW can therefore be effectively used to produce ceramic composites with local microstructures to enhance their mechanical properties or create unusual shapes. Thanks to the large microstructural design space offered by M-DIW, a variety of structures can be explored, elevating the 3D printing method to a 4D printing approach. However, a true fabrication method should offer tunability in chemistry. Therefore, in the next section we show that our M-DIW printing is not limited to alumina microplatelets only but can be applied to other types of microplatelets. This is another considerable advantage in comparison to other printing approaches. To demonstrate this, we used graphite microplatelets instead of alumina and produced functional materials with anisotropic properties.

3.5. Applying M-DIW to other microplatelets compositions

We propose to use M-DIW to fabricate graphite composites. Graphite is an interesting material for its electrical conductivity as well as relatively high energy density for applications in batteries, for example. Anodes with graphite microplatelets aligned perpendicularly to the current collector could promote the diffusion of charge carriers by shortening the tortuosity route and thereby improve the specific charge [45]. We therefore used commercial graphite microplatelets of a diameter of 1–12 μm and of a thickness of 50–300 nm (see Fig. S17 for the size distributions). Thanks to the oxygen functional groups present at the surface of the graphite microplatelets (see Fig. S18), positively charged SPIONs could be adsorbed on their surface. Here, due to the adsorption capability of Fe_3O_4, 7 vol% SPIONs were coated on graphite to make the magnetically responsive graphite microplatelets (mGr). To use M-DIW to print oriented graphite-based materials, we applied the same protocol as for the alumina microplatelets to find the optimum ink composition and measured some basic properties of materials obtained (Fig. 6).

First, dilute amounts of mGr were suspended in the resin with increasing fumed silica content and their ability to orient was observed under optical microscopy (Fig. 6A). We found that these mGr microplatelets could align in the resin with up to 7 wt% SiO_2, corresponding to a background viscosity of 100 Pa·s. It took them about 25 s to align. This is quite different from the mAl_2O_3 microplatelets. The higher alignment time is a result of the lower SPIONs coating. Indeed, graphite had less ability to adsorb SPIONs as compared to Al_2O_3 and the SPIONs coating could not be increased further. However, interestingly, the mGr microplatelets could align in the same viscous solutions as the mAl_2O_3 microplatelets. This is likely because these resin-silica suspensions had G'<G'' confirming that the stiffness of the liquid is the main hindrance to the alignment.

As for mAl_2O_3, we chose 4 wt% SiO_2 suspended in water as a background liquid for the ink and varied the wt% of mGr. We found that 10 wt% of mGr, corresponding to 4.3 vol%, yielded a suitable ink with a viscosity of 78 Pa·s as well as the yield stress of 2.5 Pa (see Fig S19 for rheological data). The alignment time in 4 wt% SiO_2 was less than 5 s, thereby satisfying the 3D printing temporal requirements of Eq. 1. With this ink, parts with as desired microstructures could be printed (Figs. 6B and S20). Similar to the alumina ink, lattice structures and other 3D shapes could be printed with high resolution and exhibited magnetic attraction (Fig. 6C). Also, the graphite composites exhibited anisotropic electrical conductivities as expected from the microstructure (Fig. 6D). For instance, the electrical conductivity measured using four-point probes on the surface of horizontally aligned 3D printed composite was 5 S/m, which was higher than on the vertically aligned samples. Furthermore, after reduction using heat treatment at 1050 ^{o}C in Argon, the electrical conductivity increased by almost 5 times, up to 26 S/m and showed high anisotropy. As compared to other 3D printed graphite materials, not only can M-DIW control the orientation, but the conductivity achieved was also higher and showed anisotropy. For example, graphite epoxy composites with a low conductivity of 0.1 S/m have been achieved using DIW [46], or graphite-PDMS with a conductivity of 140 μm S/m [47]. Low electrical conductivity can be interesting for sensing applications whereas high conductivity can be used for electronic devices, batteries, etc. With our high electrical and magnetic properties, we can fabricate magnetically controlled switches (Fig. 6E). In short, a conductive composite was 3D printed to join two copper wires powering a LED. Approaching a magnet attracted the composite, thereby disconnecting the circuit. Thanks to 3D printing, more complex 3D designs can also be made. Other concrete applications can be imagined for this type of functional inks, such as for 3D electronic packaging with high local thermal conductivity [1], or for anodes in batteries [45], among others. With these graphite composites, we illustrate how M-DIW can be effectively applied to composite inks containing functionalized microplatelets of various chemistries, following the same ink design and optimization procedure.

4. Conclusion

We introduced M-DIW as a universal, facile, cost and time-efficient 3D printing method for creating microstructured composite and ceramic materials of various chemistries and functionalities. The alignment quality obtained was similar to that obtained using other magnetically oriented methods, with a misorientation of about 20°, depending on the aspect ratio of the microplatelets used [36]. The printing time was greatly improved as compared to other magnetic printing methods thanks to the continuous deposition of the ink. In previous magnetic 3D printing, it took about 5 hrs to print 51 layers, using M-DIW, it would take only 1.1 hrs approximately. As a porous substrate was used to quickly remove the water from the deposited ink to solidify it and maintain shape fidelity, the thickness of our print has limitations to a few centimeters. To improve the size of the printed parts, external heat can be applied in conjunction with the porous substrate. Also, to further accelerate the printing, a larger magnet could be used to distribute the magnetic field over a larger area to align the microplatelets over a larger area. Depending on the intended microstructural design, there may be a trade-off between achieving orientations in local areas of small dimensions and high printing speed. With the ink optimization principles presented here, inks compositions with other microplatelets chemistries and dimensions could be developed by tuning the magnetic coating, concentration, and viscosity of the background liquid. Although we focused on high solid loading materials, soft composites with microstructure could a fortiori be obtained as well by adding a polymer or hydrogel in the ink, or by using a low concentration in the ink and infiltrating the printed material after its drying.

The proof-of-concept printed multifunctional materials were ceramics and conductive composites. The performance of these materials was similar to that of others obtained with some other techniques.

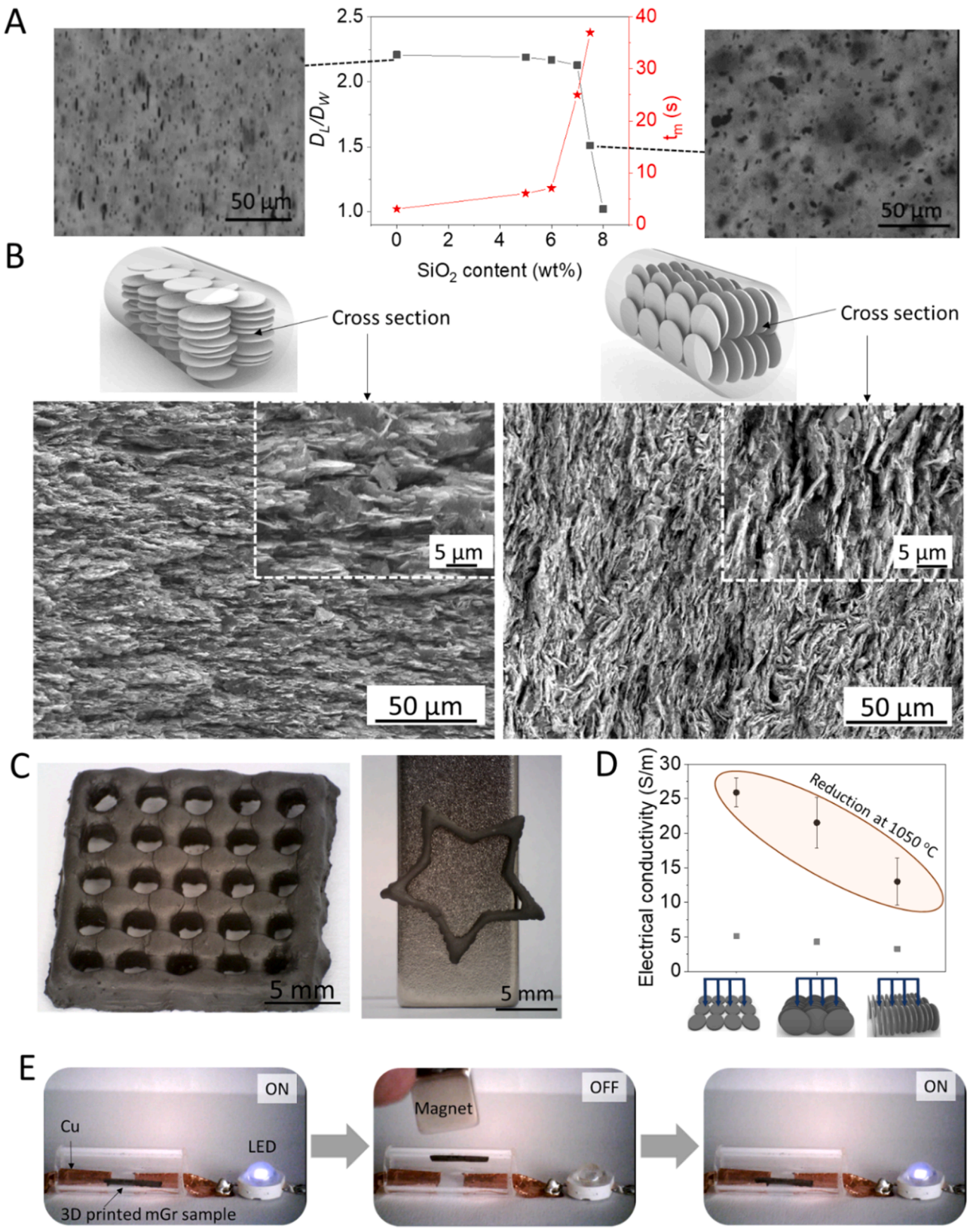

Fig. 6. M-DIW of graphite-based composites. (A) Alignment degree D_L/D_W (black) and t_m (red) for graphite microplatelets functionalized with 7 vol% SPIONs and dispersed in the resin with various SiO_2 content. The optical images show aligned mGr in low SiO_2 content (left) and non-aligned mGr in the resin with 7.5 wt% SiO_2 (right). (B) Schematics and corresponding electron micrographs showing the microstructure obtained in 3D printed graphite composites, with horizontal (left) and vertical (right) orientation. (C) Pictures of macroscopic 3D printed structures: a lattice structure made from 30 layers and a star shape made of 10 layers which has been attracted to a magnet. (D) Electrical conductivity of 3D printed graphite composites measured on the surface of sample with horizontal alignment, vertical alignment parallel to the measured probes' direction, vertical alignment perpendicularly to the measured probes' direction, before (grey, squares) and after reduction (black, circles). (E) Illustration of a 3D printed graphite-based composite in a magnetically controlled switch application.

However, we obtained them in 3D shapes and with a simple and tunable 3D printing method which is advantageous for applications. Further enhancement of the performance could be achieved by optimizing the inks in this direction. This was outside the scope of this work but could be envisaged easily. For example, for the densification of the ceramics, alumina nanoparticles could be added into the ink to increase the grain growth during the sintering. Alternatively, oxides acting as flux, such as CaO could be added. These optimizations could enable the 3D printing of nacre-like alumina with high strength and toughness [44]. For the conductive inks, the shape and exfoliation of the graphite microplatelets could be tuned to improve their percolation. Also, other high performance 2D nanomaterials could be used instead. Due to the coating with SPIONs, all the printed materials have magnetic properties, which could be removed by dissolving the iron oxide using orthophosphoric acid. Finally, the automatization and programming of the magnetic field orientation using a Computer Aided Design interface simultaneously as the DIW would be the important next step to transpose M-DIW for the fabrication of parts for the industry.

Overall, the composite and ceramic materials obtained by M-DIW have tunable composition and microstructure, which significantly expands the design space possibly for the creation of complex materials. This is promising for a large range of applications in robotics with actuators and sensors to electronics with supercapacitors, and batteries, for example.

CRediT authorship contribution statement

Fan Jingbo: Writing – review & editing, Investigation, Data curation. **Chan Xin Ying:** Writing – review & editing, Methodology, Investigation, Data curation. **Le Ferrand Hortense:** Writing – review & editing, Supervision, Funding acquisition, Conceptualization. **Guan Lizhi:** Writing – original draft, Visualization, Investigation, Data curation, Conceptualization.

Declaration of Competing Interest

The authors declare that they have no known competing financial interests or personal relationships that could have appeared to influence the work reported in this paper.

Data availability

Data will be made available on request.

Acknowledgments

This research was funded by the National Research Foundation of Singapore, Singapore (Award NRFF12 2020–0002). We acknowledge Prof Li Hong for the use of the furnace and Yong Mei Yoke for helping with the scanning electron microscopy. We are thankful to Rohit Pratyush Behera, Dr. Zehui Du for the useful discussions and Huanlong Hu, Hongying He for their help with the XRD.

Declaration of interests

All authors declare they have no competing interests.

Appendix A. Supporting information

Supplementary data associated with this article can be found in the online version at doi:10.1016/j.addma.2022.103373.

References

[1] H. He, W. Peng, J. Liu, X.Y. Chan, S. Liu, L. Lu, H.L. Ferrand, Microstructured BN composites with internally designed high thermal conductivity paths for 3D electronic packaging, Adv. Mater. 2205120.
[2] R.M. Erb, R. Libanori, N. Rothfuchs, A.R. Studart, Composites reinforced in three dimensions by using low magnetic fields, Science 335 (6065) (2012) 199–204.
[3] A.R. Studart, R.M. Erb, Bioinspired materials that self-shape through programmed microstructures, Soft Matter 10 (9) (2014) 1284–1294.
[4] R.P. Behera, H. Le, Impact-resistant materials inspired by the mantis shrimp's dactyl club, Matter 4 (9) (2021) 2831–2849.
[5] H. Le Ferrand, F. Bouville, T.P. Niebel, A.R. Studart, Magnetically assisted slip casting of bioinspired heterogeneous composites, Nat. Mater. 14 (11) (2015) 1172–1179.
[6] Y. Wang, S.E. Naleway, B. Wang, Biological and bioinspired materials: Structure leading to functional and mechanical performance, Bioactive, Materials 5 (4) (2020) 745–757.
[7] L.Z. Guan, M.C. Gutiérrez, M.J. Roldán-Ruiz, R. Jiménez, M.L. Ferrer, F. del Monte, Highly Efficient and Recyclable Carbon-Nanofiber-Based Aerogels for Ionic Liquid–Water Separation and Ionic Liquid Dehydration in Flow-Through Conditions, Adv. Mater. 31 (39) (2019) 1903418.
[8] Z. Yuan, X. Xiao, J. Li, Z. Zhao, D. Yu, Q. Li, Self-assembled graphene-based architectures and their applications, Adv. Sci. 5 (2) (2018) 1700626.
[9] Z. Xu, H. Sun, X. Zhao, C. Gao, Ultrastrong fibers assembled from giant graphene oxide sheets, Adv. Mater. 25 (2) (2013) 188–193.
[10] S. Liu, K. Hu, M. Cerruti, F. Barthelat, Ultra-stiff graphene oxide paper prepared by directed-flow vacuum filtration, Carbon 158 (2020) 426–434.
[11] A. Amini, A. Khavari, F. Barthelat, A.J. Ehrlicher, Centrifugation and index matching yield a strong and transparent bioinspired nacreous composite, Science 373 (6560) (2021) 1229–1234.
[12] Y. Xia, T.S. Mathis, M.-Q. Zhao, B. Anasori, A. Dang, Z. Zhou, H. Cho, Y. Gogotsi, S. Yang, Thickness-independent capacitance of vertically aligned liquid-crystalline MXenes, Nature 557 (7705) (2018) 409–412.
[13] C.A. Martin, J.K.W. Sandler, A.H. Windle, M.K. Schwarz, W. Bauhofer, K. Schulte, M.S.P. Shaffer, Electric field-induced aligned multi-wall carbon nanotube networks in epoxy composites, Polymer 46 (3) (2005) 877–886.
[14] R.D. Farahani, M. Dubé, D. Therriault, Three-Dimensional Printing of Multifunctional Nanocomposites: Manufacturing Techniques and Applications, Adv. Mater. 28 (28) (2016) 5794–5821.
[15] A. Schwab, R. Levato, M. D'Este, S. Piluso, D. Eglin, J. Malda, Printability and Shape Fidelity of Bioinks in 3D Bioprinting, Chem. Rev. 120 (19) (2020) 11028–11055.
[16] W. Xu, S. Jambhulkar, D. Ravichandran, Y. Zhu, M. Kakarla, Q. Nian, B. Azeredo, X. Chen, K. Jin, B. Vernon, D.G. Lott, J.L. Cornella, O. Shefi, G. Miquelard-Garnier, Y. Yang, K. Song, 3D Printing-Enabled Nanoparticle Alignment: A Review of Mechanisms and Applications, Small 17 (45) (2021) 2100817.
[17] A. Sydney Gladman, E.A. Matsumoto, R.G. Nuzzo, L. Mahadevan, J.A. Lewis, Biomimetic 4D printing, in: Nat. Mater, 15, 2016, pp. 413–418.
[18] E. Feilden, C. Ferraro, Q. Zhang, E. García-Tuñón, E. D'Elia, F. Giuliani, L. Vandeperre, E. Saiz, 3D printing bioinspired ceramic composites, Sci. Rep. 7 (1) (2017) 13759.
[19] Y. Yang, Z. Chen, X. Song, Z. Zhang, J. Zhang, K.K. Shung, Q. Zhou, Y. Chen, Biomimetic anisotropic reinforcement architectures by electrically assisted nanocomposite 3D printing, Adv. Mater. 29 (11) (2017) 1605750.
[20] J.J. Martin, B.E. Fiore, R.M. Erb, Designing bioinspired composite reinforcement architectures via 3D magnetic printing, Nat. Commun. 6 (1) (2015) 8641.
[21] G.M. Gratson, M. Xu, J.A. Lewis, Direct writing of three-dimensional webs, Nature 428 (6981) (2004), 386-386.
[22] T.E. Greenwood, S.E. Hatch, M.B. Colton, S.L. Thomson, 3D printing low-stiffness silicone within a curable support matrix, Addit. Manuf. 37 (2021), 101681.
[23] P. Dee, S. Tan, H.L. Ferrand, Fabrication of microstructured calcium phosphate ceramics scaffolds by material extrusion-based 3D printing approach, Int. J. Bioprinting 8 (2) (2022) 551.
[24] Q. Zhang, F. Zhang, S.P. Medarametla, H. Li, C. Zhou, D. Lin, 3D printing of graphene aerogels, Small 12 (13) (2016) 1702–1708.
[25] T.P. Niebel, F.J. Heiligtag, J. Kind, M. Zanini, A. Lauria, M. Niederberger, A. R. Studart, Multifunctional microparticles with uniform magnetic coatings and tunable surface chemistry, RSC Adv. 4 (107) (2014) 62483–62491.
[26] G. Korneva, H. Ye, Y. Gogotsi, D. Halverson, G. Friedman, J.-C. Bradley, K. G. Kornev, Carbon Nanotubes Loaded with Magnetic Particles, Nano Lett. 5 (5) (2005) 879–884.
[27] D. Kokkinis, M. Schaffner, A.R. Studart, Multimaterial magnetically assisted 3D printing of composite materials, Nat. Commun. 6 (1) (2015) 8643.
[28] H. Le Ferrand, F. Bouville, A.R. Studart, Design of textured multi-layered structures via magnetically assisted slip casting, Soft Matter 15 (19) (2019) 3886–3896.
[29] X.Y. Chan, C. Chua, S. Tan, H. Le, Ferrand, Energy dissipation in composites with hybrid nacre-like helicoidal microstructures, Compos, B. Eng. 232 (2022), 109608.
[30] V.H.Y. Chou, W.C. Liu, M. Wittwer, H. Le Ferrand, M. Seita, High-throughput microstructure and composition characterisation of microplatelet reinforced composites using directional reflectance microscopy, Acta Mater. 229 (2022), 117798.
[31] H. Le Ferrand, S. Bolisetty, A.F. Demirörs, R. Libanori, A.R. Studart, R. Mezzenga, Magnetic assembly of transparent and conducting graphene-based functional composites, Nat. Commun. 7 (1) (2016) 12078.
[32] J.J. Martin, M.S. Riederer, M.D. Krebs, R.M. Erb, Understanding and overcoming shear alignment of fibers during extrusion, Soft Matter 11 (2) (2015) 400–405.

[33] R.M. Erb, J. Segmehl, M. Charilaou, J.F. Löffler, A.R. Studart, Non-linear alignment dynamics in suspensions of platelets under rotating magnetic fields, Soft Matter 8 (29) (2012) 7604–7609.
[34] J.W. Boley, W.M. van Rees, C. Lissandrello, M.N. Horenstein, R.L. Truby, A. Kotikian, J.A. Lewis, L. Mahadevan, Shape-shifting structured lattices via multimaterial 4D printing, Proc. Natl. Acad. Sci. U. S. A. 116(42), 2019: 20856–20862.
[35] S. Puthanveetil, W.C. Liu, K.S. Riley, A.F. Arrieta, H. Le, Ferrand, Programmable multistability for 3D printed reinforced multifunctional composites with reversible shape change, Compos. Sci. Technol. 217 (2022), 109097.
[36] H. Le Ferrand, Magnetic slip casting for dense and textured ceramics: A review of current achievements and issues, J. Eur. Ceram. Soc. 41 (1) (2021) 24–37.
[37] Q. Zhang, S. Rastogi, D. Chen, D. Lippits, P.J. Lemstra, Low percolation threshold in single-walled carbon nanotube/high density polyethylene composites prepared by melt processing technique, Carbon 44 (4) (2006) 778–785.
[38] F.L. Bargardi, H. Le Ferrand, R. Libanori, A.R. Studart, Bio-inspired self-shaping ceramics, Nat. Commun. 7 (1) (2016) 13912.
[39] I. Corni, T.J. Harvey, J.A. Wharton, K.R. Stokes, F.C. Walsh, R.J.K. Wood, A review of experimental techniques to produce a nacre-like structure, Bioinspir. Biomim. 7 (3) (2012), 031001.
[40] G.M. Luz, J.F. Mano, Biomimetic design of materials and biomaterials inspired by the structure of nacre, Philos. Trans. R. Soc. A 367 (1893) (2009) 1587–1605.
[41] J. Liu, Q. Li, M. Huo, X. Zhang, X. Yue, J. Liang, J. Li, Microstructure and mechanical properties of 3D-printed nano-silica reinforced alumina cores, Ceram. Int. 48 (20) (2022) 30282–30293.
[42] A.-K. Hofer, I. Kraleva, R. Bermejo, Additive manufacturing of highly textured alumina ceramics, Open Ceram. 5 (2021), 100085.
[43] W. Liu, M. Li, J. Nie, C. Wang, W. Li, Z. Xing, Synergy of solid loading and printability of ceramic paste for optimized properties of alumina via stereolithography-based 3D printing, J. Mater. Res. Technol. 9 (5) (2020) 11476–11483.
[44] F. Bouville, E. Maire, S. Meille, B. Van de Moortèle, A.J. Stevenson, S. Deville, Strong, tough and stiff bioinspired ceramics from brittle constituents, Nat. Mater. 13 (5) (2014) 508–514.
[45] J. Billaud, F. Bouville, T. Magrini, C. Villevieille, A.R. Studart, Magnetically aligned graphite electrodes for high-rate performance Li-ion batteries, Nat. Energy 1 (8) (2016) 16097.
[46] R. Haney, P. Tran, E.B. Trigg, H. Koerner, T. Dickens, S. Ramakrishnan, Printability and performance of 3D conductive graphite structures, Addit. Manuf. 37 (2021), 101618.
[47] A. Nag, S. Feng, S.C. Mukhopadhyay, J. Kosel, D. Inglis, 3D printed mould-based graphite/PDMS sensor for low-force applications, Sens. Actuator A Phys. 280 (2018) 525–534.